GRASS: Ground-level Recognition of Aromatic Species Spectrum at the Network Far-Edge Onboard UAVs

A. Caruso*, C. Grasso*, D. Condorelli†, G. A. Malfa†, R. Acquaviva†, G. Schembra*
*DIEEI and CNIT Research Unit, University of Catania, Italy
†DSFS and CERNUT, University of Catania, Italy

***Abstract*—Aromatic and officinal plants play a key role in ecological systems and industrial applications, making their large-scale monitoring increasingly relevant. However, their automatic identification in natural environments remains challenging due to visual similarity, co-occurrence, and environmental variability. This paper presents GRASS (Ground-level Recognition of Aromatic Species Spectrum), a spectral-driven framework for plant classification based on RGB and multispectral UAV data, designed for lightweight on-board inference at the network far edge. The approach relies on the extraction of compact class-specific spectral signatures from a limited set of annotated samples, enabling data-efficient training without the need for large datasets. During inference, classification is performed through a computationally efficient spectral decision mechanism, avoiding the overhead of traditional machine learning models and making the method suitable for real-time execution on resource-constrained UAV platforms. By combining RGB and multispectral information, GRASS captures both morphological and physiological characteristics of vegetation, improving class separability in complex scenarios. Experimental results demonstrate that the proposed approach achieves high accuracy while maintaining low computational complexity, making it well-suited for on-device and pervasive intelligence applications.**

***Index Terms*—UAV, On-Device AI, Far-Edge Computing, Multispectral Imaging, Spectral Modeling, Lightweight Inference**

I. Introduction

Aromatic and officinal plants constitute a valuable natural resource with significant ecological, economic, and pharmacological relevance. They are widely used in therapeutic applications and in the production of pharmaceuticals, cosmetics, and plant-derived products, while also playing a key role in biodiversity preservation and ecosystem functioning [1], [2]. Their identification and monitoring are therefore essential for sustainable management and large-scale environmental analysis. Many of these species coexist in heterogeneous environments, both in cultivated and spontaneous vegetation, increasing the complexity of their detection [3]. Traditional ground-based surveys are often labor-intensive, time-consuming, and limited in spatial coverage. For this reason, remote sensing techniques have gained increasing attention, enabling systematic observations over wide areas with high spatial resolution [4], [5]. Among sensing platforms, Unmanned Aerial Vehicles (UAVs) represent a flexible and cost-effective solution, supporting high-resolution data acquisition and multi-modal sensing, including red-green-blue (RGB) and multispectral imagery [6], [7]. Multispectral data complement RGB images by measuring reflectance in selected spectral bands, such as Green, Red, Red-Edge, and Near Infrared, which are related to vegetation physiological properties. These capabilities have fostered UAV adoption in several domains such as precision agriculture, environmental monitoring, and biodiversity assessment [8]. Several approaches have been proposed for UAV-based plant species recognition. Many rely on RGB imagery combined with machine learning or deep learning techniques, achieving promising results in complex environments [9]. Other works exploit multispectral data to leverage vegetation reflectance properties for classification [10], [11]. However, these approaches often require large annotated datasets and computationally demanding models, which may limit their applicability in resource-constrained UAV on-board systems and in deployments where wireless connectivity to ground or cloud infrastructure is intermittent or bandwidth-limited. In this context, there is a growing need for lightweight and data-efficient solutions capable of moving part of the inference process directly to UAV platforms at the network far edge [12], [13]. Processing data on-board can reduce the need to continuously transmit high-resolution RGB and multispectral imagery, while allowing compact classification outputs or alerts to be exchanged with ground or edge infrastructure when connectivity is available.

To address these challenges, this paper introduces GRASS (Ground-level Recognition of Aromatic Species Spectrum), a spectral-driven framework for plant species recognition based on the combined use of RGB and multispectral UAV imagery. The proposed approach departs from data-intensive learning paradigms by relying on compact spectral descriptors extracted from a limited set of annotated samples. This reduces the annotation and training effort while preserving discriminative capability in the considered scenario.

During inference, classification is performed through a lightweight spectral decision mechanism based on class statistics, without requiring iterative model training or large learned weights. RGB and multispectral data are jointly exploited to capture complementary information: morphological charac-

ISBN 978-3-903176-82-9

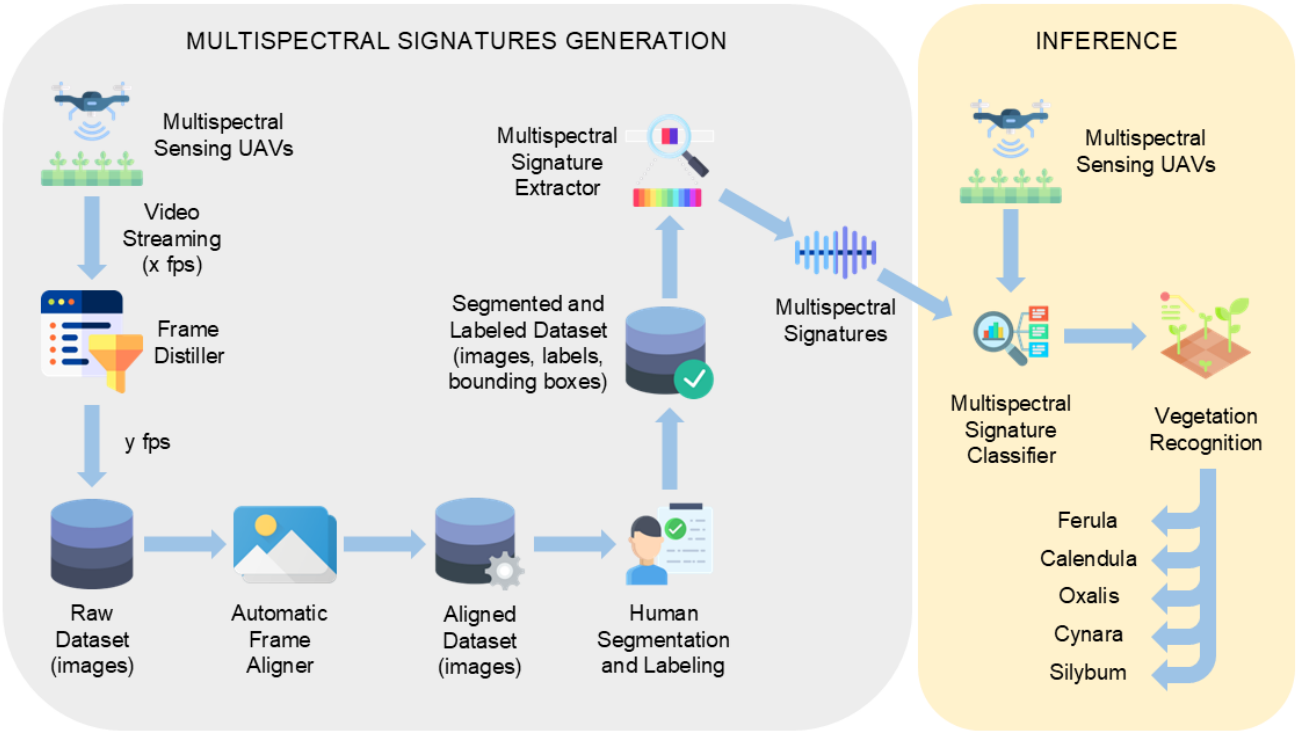

Fig. 1: Reference architecture

teristics from RGB imagery and physiological properties from multispectral bands. This integration improves discrimination among species with similar visual appearance or overlapping spectral responses, which are common in complex natural environments.

The remainder of this paper is organized as follows. Section II describes the proposed framework and methodology. Section III presents the experimental setup and dataset. Section IV discusses the obtained results, while Section V concludes the paper and outlines future research directions.

II. Reference Architecture

The general architecture of the proposed system is depicted in Fig. 1. The framework is organized into two main stages, both provided by edge and far-edge sensing and computing facilities deployed onboard UAVs: a multispectral analysis phase to derive compact spectral representations of the target species, and a lightweight inference phase designed for onboard UAV execution. The *Multispectral Sensing UAVs* acquire aerial imagery through RGB and multispectral cameras. Each acquisition produces a sequence of frames composed of RGB channels and additional spectral bands, such as Green (G), Red (R), Red-Edge (RE), and Near Infrared (NIR). To reduce data redundancy and limit on-board processing, a *Frame Distiller* module is applied to the incoming video stream. Consecutive frames are compared using a similarity metric, and only sufficiently dissimilar frames are retained. Let I_t and I_{t-1} denote two consecutive frames. The similarity score is defined as:

$$\text{SSID}(I_t, I_{t-1}) = \mathcal{S}(I_t, I_{t-1}) \tag{1}$$

where $\mathcal{S}(\cdot)$ represents a similarity function, such as the Structural Similarity Index (SSIM) or a normalized correlation measure. A frame I_t is retained only if

$$\text{SSID}(I_t, I_{t-1}) < \tau \tag{2}$$

where τ is a predefined threshold. This mechanism reduces redundancy while preserving relevant scene variations, enabling more efficient downstream processing.

The selected frames are stored as a *Raw Dataset* consisting of multispectral image sets. Each frame includes multiple spectral images corresponding to the available bands. Before further processing, the images undergo an *Automatic Frame Alignment* procedure to compensate for spatial misalignment between RGB and multispectral sensors mounted onboard the same UAV. This step is performed using a feature-based approach based on the Scale-Invariant Feature Transform (SIFT). Since RGB and multispectral images have different resolutions and fields of view, lower-resolution copies of both images are first generated to reduce the computational cost of keypoint extraction and matching. The matched keypoints are then used to estimate the alignment transformation. Finally, the RGB image, which covers a wider field of view, is cropped to the multispectral reference size, yielding spatially coherent RGB and multispectral data on a common image domain, as shown in Fig. 2. After alignment, the dataset is annotated using a segmentation tool. A domain expert identifies plant regions of interest by drawing polygons on RGB images, assigning a class label to each region (Fig. 3). Unlike conventional machine learning approaches, which typically require large annotated datasets, the proposed method relies on

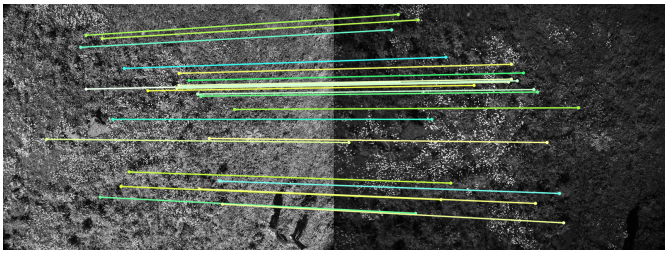

Fig. 2: RGB-Multispectral SIFT Alignment

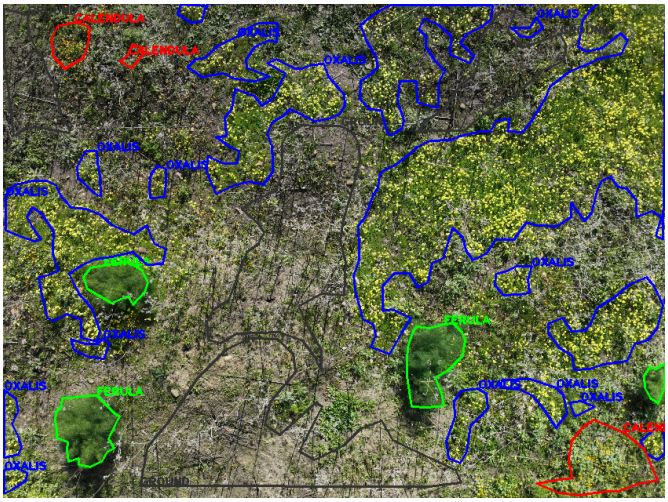

Fig. 3: Example of segmented and annotated image

spectral characterization and therefore requires only a limited number of annotated samples per class. This significantly reduces the training effort and enables rapid deployment in new environments. From the annotated dataset, spectral features are extracted to construct representative multispectral signatures for each class. Each pixel is described by a spectral vector combining RGB and multispectral information:

$$\underline{x} = [x_R, x_G, x_B, x_{G'}, x_{R'}, x_{RE'}, x_{NIR'}] \tag{3}$$

where x_R, x_G, and x_B denote RGB channels, while $x_{G'}$, $x_{R'}$, $x_{RE'}$, and $x_{NIR'}$ correspond to multispectral bands. The dimensionality of the spectral vector is $d = 7$. Let N_c be the number of annotated polygons belonging to class c, and let k denote a generic polygon. For each annotated polygon P_k, a binary mask M_k is defined as:

$$M_k(\underline{\hat{x}}) = \begin{cases} 1 & \text{if } \underline{\hat{x}} \in P_k \\ 0 & \text{otherwise} \end{cases} \tag{4}$$

where $\underline{\hat{x}}$ represents a generic pixel.

Spectral vectors belonging to the same class are aggregated to compute statistical descriptors defining the class spectral signature. The mean spectral vector is given by:

$$\underline{\mu}_c = [\mu_{c,R}, \mu_{c,G}, \mu_{c,B}, \mu_{c,G'}, \mu_{c,R'}, \mu_{c,RE'}, \mu_{c,NIR'}] = \\ = \frac{1}{N_c} \sum_{k=1}^{N_c} \left(\frac{1}{N_k} \sum_{\underline{x} \in P_k} \underline{x} \right) \tag{5}$$

where N_k is the number of pixels in polygon P_k. This formulation ensures that each annotated region contributes equally to the class representation.

Minimum and maximum values are also computed for each spectral band, and the covariance matrix is estimated as:

$$\mathbf{\Sigma_c} = \frac{1}{N_c} \sum_{k=1}^{N_c} \left(\frac{1}{N_k - 1} \sum_{\underline{x} \in P_k} (\underline{x} - \underline{\mu}_c)(\underline{x} - \underline{\mu}_c)^T \right) \tag{6}$$

These parameters define a compact spectral model for each class, enabling efficient classification without the need for data-intensive training procedures or large learned model weights. During inference, the extracted spectral signatures are used to classify new observations directly on-board. For each pixel $\underline{x}$, its similarity with class c is evaluated using the *Mahalanobis distance*:

$$d_{Mah}(\underline{x}, c) = (\underline{x} - \underline{\mu}_c)^T \mathbf{\Sigma_c}^{-1} (\underline{x} - \underline{\mu}_c) \tag{7}$$

A penalty term is introduced to account for deviations from the expected spectral range:

$$R(\underline{x}, c) = \sqrt{\sum_{j=1}^{d} w_j \, r_j(\underline{x}, c)^2} \tag{8}$$

where

$$r_j(\underline{x}, c) = \frac{1}{\Delta_{c,j}} \begin{cases} m_{c,j}^{\min} - x_j & \text{if } x_j < m_{c,j}^{\min} \\ x_j - m_{c,j}^{\max} & \text{if } x_j > m_{c,j}^{\max} \\ 0 & \text{otherwise} \end{cases} \tag{9}$$

with $\Delta_{c,j} = m_{c,j}^{\max} - m_{c,j}^{\min}$.

The final classification score is defined as:

$$S(\underline{x}, c) = \alpha \, d_{Mah}(\underline{x}, c) + \beta \, R(\underline{x}, c) \tag{10}$$

Each pixel is assigned to the class minimizing the score:

$$\hat{c}(\underline{x}) = \arg\min_c S(\underline{x}, c) \tag{11}$$

This lightweight decision mechanism enables fast inference compared to conventional machine learning models, making it suitable for real-time execution on resource-constrained UAV platforms. The resulting classification map provides the spatial distribution of plant species within the observed area.

III. Experimental Setup

To evaluate the effectiveness of the proposed framework, experiments were conducted on multispectral UAV imagery acquired over natural vegetation areas containing different plant species. The study considers five aromatic and officinal species for automatic recognition: *Ferula communis* L., *Calendula arvensis* L., *Oxalis pes-caprae* L., *Cynara cardunculus* L., and *Silybum marianum* (L.) Gaertn. These species were selected due to both their pharmacological relevance and their presence in the investigated area. Representative examples are shown in Fig. 4.

Ferula communis L. (Apiaceae), commonly known as giant fennel, is characterized by a large taproot and tall stems with

Ferula communis L. | *Calendula arvensis* L. | *Oxalis pes caprae* L. | *Cynara cardunculus* L. | *Silybum marianum* L. Gaertn.

Fig. 4: Specimens of the five target species

yellow umbels [14], making it relatively distinguishable in aerial imagery.

Calendula arvensis L. (Asteraceae), or field marigold, is a small herbaceous plant with yellow-orange flowers [15], whose limited size and dense distribution make detection challenging.

Oxalis pes-caprae L. (Oxalidaceae) forms dense ground cover with trifoliate leaves and yellow flowers [16]. Its appearance is often similar to *C. arvensis*, especially from aerial views.

Cynara cardunculus L. (Asteraceae), known as wild cardoon, exhibits large leaves and robust stems [17], while *Silybum marianum* (L.) Gaertn. (Asteraceae), or milk thistle, presents distinctive white-marbled leaves and similar structural features [18]. These similarities can lead to classification ambiguities.

The considered species define a challenging scenario, including both visually distinctive plants and species with overlapping morphological and spectral characteristics. In particular, pairs such as *C. arvensis* and *O. pes-caprae*, as well as *C. cardunculus* and *S. marianum*, are difficult to distinguish when relying on a single data modality. To better model the scene context, two additional classes were included during annotation: *Grass*, representing generic vegetation, and *Ground*, corresponding to bare soil. The dataset was acquired using a DJI Mavic 3M UAV equipped with one RGB camera and four multispectral sensors operating in the Green (G), Red (R), Red Edge (RE), and Near Infrared (NIR) bands. RGB imagery provides high-resolution information on vegetation morphology (shape, texture, and color), with channels covering Blue (450–495 nm), Green (495–570 nm), and Red (620–750 nm). Multispectral sensors, instead, capture reflectance at specific wavelengths, enabling the analysis of plant physiological properties. In particular, the multispectral sensors operate at central wavelengths of Green (560 $\pm$ 10 nm), Red (650 $\pm$ 10 nm), Red Edge (730 $\pm$ 10 nm), and Near Infrared (840 $\pm$ 10 nm). These bands provide complementary information related to chlorophyll absorption, vegetation health, and leaf structure, supporting more accurate species discrimination. Data acquisition was performed through pre-programmed UAV missions at an altitude of approximately 12 meters, following a serpentine trajectory to ensure uniform coverage. All missions were conducted under stable illumination conditions (clear weather, between 12:00 and 14:00) to minimize lighting variability.

The RGB camera produced images with a resolution of 5280×3956 pixels, while multispectral sensors generated TIFF images of 2592×1944 pixels. A total of 5430 images were collected across three UAV missions, corresponding to 1086 frames (each composed of one RGB and four multispectral images). Only a limited subset of frames was manually annotated to derive spectral signatures, demonstrating the data-efficient nature of the proposed approach, which does not require large-scale labeled datasets. A summary of the acquisition campaigns is reported in Table I.

TABLE I: Summary of UAV acquisition missions

Mission	Duration	Images	Frames	Usage
1	13 min 06 s	1825	365	Training
2	15 min 26 s	2150	430	Training
3	10 min 30 s	1455	291	Test

IV. Numerical Results

For the experimental evaluation, the data collected during the first two missions were used to build the training dataset and extract spectral representations of the considered plant species, while the third mission was used as an independent test set. A selected subset of training images was manually annotated following the procedure described in Section II (see Fig. 3). The annotated regions were used to derive class-specific spectral signatures for all classes, reducing the labeling effort with respect to approaches that require large-scale labeled datasets. From the annotated data, class-specific spectral signatures were estimated by aggregating pixel-level spectral responses within labeled regions, yielding compact representations in the spectral feature space. The overall workflow is illustrated in Fig. 6. Spectral profiles are constructed from the annotated data and used during inference to perform pixel-wise classification on unseen UAV imagery. Each pixel is evaluated against all class profiles through a scoring function combining a distance-based similarity to the class centroid and a penalty term accounting for deviations from the expected spectral range. The weighting parameters in (10) were set to $\alpha = 0.6$ and $\beta = 0.6$ after preliminary trials on the training missions, in order to balance the contribution of the Mahalanobis distance (7) and the range-based penalty term (8). The same values were then kept fixed for the test mission. At object level, the final classification is obtained by aggregating pixel-wise predictions within each annotated region through a majority voting strategy. This reduces the impact of local pixel-level errors and provides more stable object-level labels. The confusion matrices for the RGB, multispectral, and combined RGB+multispectral configurations are reported in Fig. 5. These matrices are computed at object level and provide a detailed view of the classification behavior across all classes. The three configurations are used to assess the contribution of each data modality within the proposed spectral framework. The RGB-only configuration shows strong dependence on visual appearance. While visually distinctive species such as *S. marianum* are correctly identified, significant confu-

sion arises among visually similar classes. In particular, *C. arvensis*, *O. pes-caprae*, and *C. cardunculus* are frequently misclassified. Background classes such as *Ground* and *Grass* are also poorly separated, indicating the limited discriminative power of RGB data alone. The multispectral configuration introduces complementary reflectance information, partially improving class separability. However, ambiguities remain, especially for species with overlapping spectral responses, and misclassifications still occur between vegetation classes and background. The combined RGB+multispectral configuration achieves a substantial improvement, as shown by the near-diagonal confusion matrix. Most classes are correctly identified, including challenging pairs such as *C. arvensis* and *O. pes-caprae*. Background classes are also more accurately separated. Residual confusion is limited to a few cases, such as partial overlap between *F. communis* and *C. arvensis*, or between *C. cardunculus* and other vegetation classes.

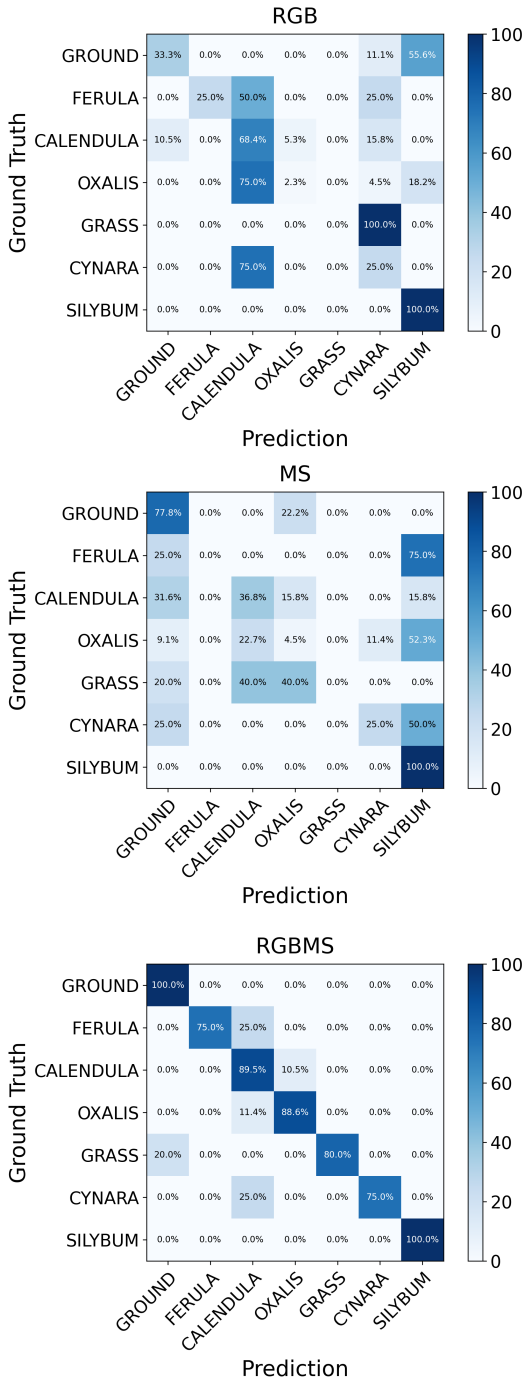

Fig. 5: Confusion matrices obtained using RGB, multispectral, and RGB+multispectral features

Table II reports precision, recall, and F1-score for each class and configuration. These results confirm the trends observed in the confusion matrices. RGB-only classification performs well only for clearly distinguishable classes, while multispectral-only classification improves the use of reflectance information but remains insufficient for reliable discrimination in all cases.

TABLE II: Classification performance metrics (object-level)

Method	Class	Precision	Recall	F1-score
RGB	*Ground*	0.31	1.00	0.48
RGB	*Ferula*	0.91	0.71	0.80
RGB	*Calendula*	0.21	0.21	0.21
RGB	*Oxalis*	0.00	0.00	0.00
RGB	*Grass*	0.00	0.00	0.00
RGB	*Cynara*	0.00	0.00	0.00
RGB	*Silybum*	1.00	1.00	1.00
MS	*Ground*	0.60	0.78	0.68
MS	*Ferula*	0.64	0.00	0.00
MS	*Calendula*	0.37	0.37	0.37
MS	*Oxalis*	0.04	0.05	0.05
MS	*Grass*	0.00	0.00	0.00
MS	*Cynara*	0.25	0.25	0.25
MS	*Silybum*	0.50	1.00	0.67
RGB+MS	*Ground*	1.00	1.00	1.00
RGB+MS	*Ferula*	0.75	0.75	0.75
RGB+MS	*Calendula*	0.89	0.90	0.89
RGB+MS	*Oxalis*	0.89	0.89	0.89
RGB+MS	*Grass*	0.80	0.80	0.80
RGB+MS	*Cynara*	0.75	0.75	0.75
RGB+MS	*Silybum*	1.00	1.00	1.00

The combined RGB+multispectral approach consistently achieves the best results across the considered classes, demonstrating that the integration of morphological and physiological information is essential for accurate plant species recognition in complex environments. Overall, the results indicate that compact spectral signatures can provide effective classification with reduced annotation effort and without relying on large learned models. Hardware-level profiling and direct comparison with lightweight neural baselines are left as future deployment-oriented evaluations.

V. Conclusions

This paper introduced GRASS (Ground-level Recognition of Aromatic Species Spectrum), a spectral-driven framework for plant species recognition based on the combined use of RGB and multispectral UAV imagery for sensing, and computing onboard UAVs for far-edge computing.

The proposed approach relies on the extraction of compact spectral descriptors from a limited set of annotated samples,

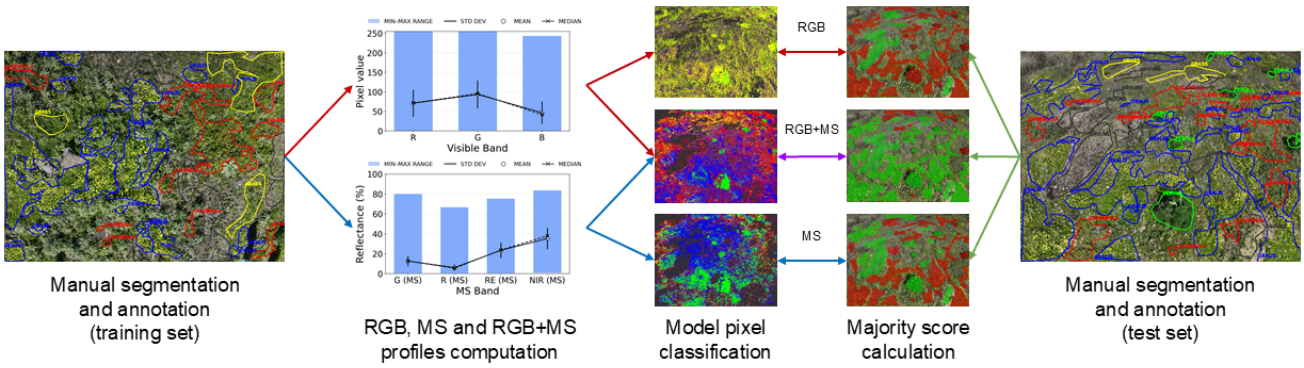

Fig. 6: Spectral profile creation and scoring method scheme

enabling data-efficient training without the need for large-scale labeled datasets. This makes the method particularly suitable for rapid deployment in real-world scenarios and for applications where annotation resources are limited.

The experimental results highlight the limitations of single-modality configurations. RGB-only approaches are effective only for visually distinctive species, while failing to discriminate plants with similar appearance. Multispectral data improve classification by incorporating reflectance information, but remain insufficient in scenarios with overlapping spectral responses. The integration of edge- and far-edge computing for RGB and multispectral information provides a substantial improvement, significantly enhancing both accuracy and robustness. The combined configuration achieves the best performance across all classes, demonstrating that morphological and physiological features provide complementary information that is essential for reliable discrimination of plant species. Compared to conventional machine learning approaches, the proposed method enables significantly reduced computational complexity during inference, making it suitable for real-time execution on resource-constrained UAV platforms and supporting the shift towards on-device and pervasive intelligence.

Future work will focus on extending the method to larger and more diverse datasets, improving robustness under varying illumination and seasonal conditions, comparing against lightweight neural baselines, and validating the framework on embedded UAV-oriented hardware.

References

[1] M. Pergola, E. De Falco, A. Belliggiano, and C. Ievoli, "The most relevant socio-economic aspects of medicinal and aromatic plants through a literature review," *Agriculture*, vol. 14, no. 3, p. 405, 2024.

[2] S. Theodoridis, E. G. Drakou, T. Hickler, M. Thines, and D. Nogues-Bravo, "Evaluating natural medicinal resources and their exposure to global change," *The Lancet Planetary Health*, vol. 7, no. 2, pp. e155–e163, 2023.

[3] T. Bhattacharjee, S. Sen, R. Chakraborty, P. K. Maurya, and A. Chattopadhyay, "Cultivation of medicinal plants: Special reference to important medicinal plants of india," in *Herbal medicine in India: Indigenous knowledge, practice, innovation and its value*. Springer, 2019, pp. 101–115.

[4] Y. Xie, Z. Sha, and M. Yu, "Remote sensing imagery in vegetation mapping: a review," *Journal of plant ecology*, vol. 1, no. 1, pp. 9–23, 2008.

[5] P. Whig, A. B. Bhatia, R. R. Nadikatu, Y. Alkali, and P. Sharma, "Gis and remote sensing application for vegetation mapping," in *Geo-environmental hazards using ai-enabled geospatial techniques and earth observation systems*. Springer, 2024, pp. 17–39.

[6] C. Grasso, R. Raftopoulos, and G. Schembra, "Tailoring fanet-based 6g network slices in remote areas for low-latency applications," in *2022 IFIP Networking Conference (IFIP Networking)*, 2022, pp. 1–6.

[7] G. Davoli, C. Grasso, A. Caruso, W. Cerroni, G. Colajanni, L. Galluccio, and G. Schembra, "A marketplace approach for service-chain deployment in a multi-layer fanet edge-computing architecture," in *2025 Integrated Communications, Navigation and Surveillance Conference (ICNS)*, 2025, pp. 1–10.

[8] C. Buzna, M. N. Horablaga, A. L. Jurjescu, F. SALA *et al.*, "Characterization of some aromatic and medicinal plants species based on uav images," *Life Science and sustainable development*, vol. 4, no. 1, pp. 101–110, 2023.

[9] G. Tariku, I. Ghiglieno, G. Gilioli, F. Gentilin, S. Armiraglio, and I. Serina, "Automated identification and classification of plant species in heterogeneous plant areas using unmanned aerial vehicle-collected rgb images and transfer learning," *Drones*, vol. 7, no. 10, p. 599, 2023.

[10] K. Musungu, T. Dube, J. Smit, and M. Shoko, "Using uav multispectral photography to discriminate plant species in a seep wetland of the fynbos biome," *Wetlands Ecology and Management*, vol. 32, no. 2, pp. 207–227, 2024.

[11] Z. Xu, X. Shen, L. Cao, N. C. Coops, T. R. Goodbody, T. Zhong, W. Zhao, Q. Sun, S. Ba, Z. Zhang *et al.*, "Tree species classification using uas-based digital aerial photogrammetry point clouds and multispectral imageries in subtropical natural forests," *International Journal of Applied Earth Observation and Geoinformation*, vol. 92, p. 102173, 2020.

[12] A. Caruso, L. Galluccio, C. Grasso, M. Ignaccolo, G. Inturri, P. Leonardi, G. Schembra, and V. Torrisi, "Advancing urban traffic monitoring in smart cities: A field experiment with uav-based system for transport planning and intelligent traffic management," in *2025 Integrated Communications, Navigation and Surveillance Conference (ICNS)*. IEEE, 2025, pp. 1–9.

[13] A. Caruso, C. Grasso, R. Raftopoulos, and G. Schembra, "Falcon: Fanet-aware learning and digital twin control framework," *Computer Communications*, vol. 251, p. 108481, 2026.

[14] R. Macrì, V. Musolino, M. Gliozzi, C. Carresi, J. Maiuolo, S. Nucera, M. Scicchitano, F. Bosco, F. Scarano, S. Ruga, M. C. Zito, L. Guarnieri, E. Bombardelli, and V. Mollace, "*Ferula* L. plant extracts and dose-dependent activity of natural sesquiterpene ferutinin: From antioxidant potential to cytotoxic effects," *Molecules*, vol. 25, no. 23, 2020.

[15] W. C. Evans, *Trease and Evans' Pharmacognosy*, ser. Health professions. Elsevier, 2014.

[16] G. A. Malfa, S. Bianchi, V. Spadaro, C. Di Giacomo, F. M. Raimondo, and R. Acquaviva, "Oxalis pes-caprae l. (oxalidaceae): From invasive concern to promising bioresource for health and sustainable applications," *Plants*, vol. 14, no. 4, 2025.

[17] R. Gebhardt and M. Fausel, "Antioxidant and hepatoprotective effects of artichoke extracts and constituents in cultured rat hepatocytes," *Toxicology in vitro*, vol. 11, no. 5, pp. 669–672, 1997.

[18] K. Flora, M. Hahn, H. Rosen, and K. Benner, "Milk thistle (silybum marianum) for the therapy of liver disease," *The American journal of gastroenterology*, vol. 93, no. 2, pp. 139–143, 1998.